Since January 2020 Elsevier has created a COVID-19 resource centre with free information in English and Mandarin on the novel coronavirus COVID-19. The COVID-19 resource centre is hosted on Elsevier Connect, the company's public news and information website.

Elsevier hereby grants permission to make all its COVID-19-related research that is available on the COVID-19 resource centre - including this research content - immediately available in PubMed Central and other publicly funded repositories, such as the WHO COVID database with rights for unrestricted research re-use and analyses in any form or by any means with acknowledgement of the original source. These permissions are granted for free by Elsevier for as long as the COVID-19 resource centre remains active.

Biomaterials 285 (2022) 121509

Contents lists available at ScienceDirect

Biomaterials

journal homepage: www.elsevier.com/locate/biomaterials

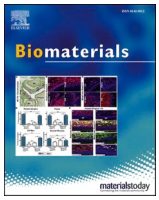

Protease inhibitor Camostat Mesyalte blocks wild type SARS-CoV-2 and D614G viral entry in human engineered miniature lungs

Tong Wu [a,b], Seyed A. Rabi [c,d], William A. Michaud [c,e], David Becerra [f], Sarah E. Gilpin [a], Mari Mino-Kenudson [a,b,g], Harald C. Ott [a,b,c,*]

[a] Massachusetts General Hospital, Center for Regenerative Medicine, Boston, MA, USA
[b] Harvard Medical School, Boston, MA, USA
[c] Massachusetts General Hospital, Department of Surgery, Boston, MA, USA
[d] Massachusetts General Hospital, Division of Cardiovascular Surgery, Boston, MA, USA
[e] Massachusetts General Hospital, Division of Surgical Oncology, Boston, MA, USA
[f] Duke University Medical Center, Department of General Surgery, USA
[g] Massachusetts General Hospital, Department of Pathology, Boston, MA, USA

A B S T R A C T

The catastrophic global effects of the SARS-CoV-2 pandemic highlight the need to develop novel therapeutics strategies to prevent and treat viral infections of the respiratory tract. To enable this work, we need scalable, affordable, and physiologically relevant models of the human lung, the primary organ involved in the pathogenesis of COVID-19. To date, most COVID-19 *in vitro* models rely on platforms such as cell lines and organoids. While 2D and 3D models have provided important insights, human distal lung models that can model epithelial viral uptake have yet to be established. We hypothesized that by leveraging techniques of whole organ engineering and directed differentiation of induced pluripotent stem cells (iPSC) we could model human distal lung epithelium, examine viral infection at the tissue level in real time, and establish a platform for COVID-19 related research *ex vivo*. In the present study, we used type 2 alveolar epithelial cells (AT2) derived from human iPSCs to repopulate whole rat lung acellular scaffolds and maintained them in extended biomimetic organ culture for 30 days to induce the maturation of distal lung epithelium. We observed emergence of a mixed type 1 and type 2 alveolar epithelial phenotype during tissue formation. When exposing our system to a pseudotyped lentivirus containing the spike of wildtype SARS-CoV-2 and the more virulent D614G, we observed progression of the infection in real time. We then found that the protease inhibitor Camostat Mesyalte significantly reduced viral transfection in distal lung epithelium. In summary, our data show that a mature human distal lung epithelium can serve as a novel moderate throughput research platform to examine viral infection and to evaluate novel therapeutics *ex vivo*.

Credit author statement

Tong Wu: Conceptualization, writing, experimental execution, data analysis and interpretation, Seyed A. Rabi: Conceptualization, viral synthesis, experimental execution, William A. Michaud: viral synthesis, David Becerra: experimental execution, Sarah E. Gilpin: conceptualization, experimental execution, Mari Mino-Kenudson: pathologic evaluation, review and editing, Harald C. Ott: conceptualization, data analysis and interpretation, manuscript writing, editing.

1. Introduction

SARS-CoV-2, the coronavirus that causes COVID-19, has claimed the lives of 5.9 million people worldwide while infecting more than 400 million patients. The necessary development time of vaccines and the emergence of SARS-CoV-2 variants highlight the significant lag and limited adaptability of the vaccine approach and the need for novel therapeutics. Among all causes of mortality, acute respiratory failure (ARF) with diffuse alveolar damage was found in most patients [1, 2]. To investigate how to intervene in this disease process and to inhibit various steps of the SARS-CoV-2 lifecycle, we need a universally available, affordable, scalable, and yet physiologically relevant platform simulating the human respiratory tract. Recently, several groups reported the application of human lung cells [3, 4], organoids [5-8], and organ-on-a-chip microfluidic systems [9-13] for the study of SARS-CoV-2 infection and induced immune responses. However, the discrepancies between these platforms and native human lung make it hard to recapitulate the pathophysiological behavior of SARS-CoV-2 virus during infection. SARS-CoV-2 employs Angiotensin-converting Enzyme-2 (ACE2) as a receptor for cellular entry [3], the expression of

* Corresponding author. Massachusetts General Hospital, Center for Regenerative Medicine, Boston, MA, USA.
E-mail address: hott@mgh.harvard.edu (H.C. Ott).

https://doi.org/10.1016/j.biomaterials.2022.121509
Received 16 June 2021; Received in revised form 8 March 2022; Accepted 1 April 2022
Available online 11 April 2022
0142-9612/© 2022 Published by Elsevier Ltd.

which is abundantly distributed throughout the human lung epithelium [14], including alveolar type 1 (AT1) and 2 (AT2) cells and small airway epithelial cells [15]. In native lungs, AT1 cells are essential for gas exchange and barrier formation, while AT2 cells secrete surfactant to support fluid balance and also function as the progenitor population for AT1 cells to maintain tissue homeostasis [16]. Autopsies have shown that both cell types are depleted in the context of SARS-CoV-2 infection, and that there is evidence of *trans*-differentiation and attempted epithelial repair between those cell types [17]. Human lung epithelial cells that exhibit AT2 cell identity can be generated from iPSCs and expand as alveolar epithelial spheres in Matrigel [18, 19]. However, the *in vitro* formation of human distal lung epithelium mimicking mature gas

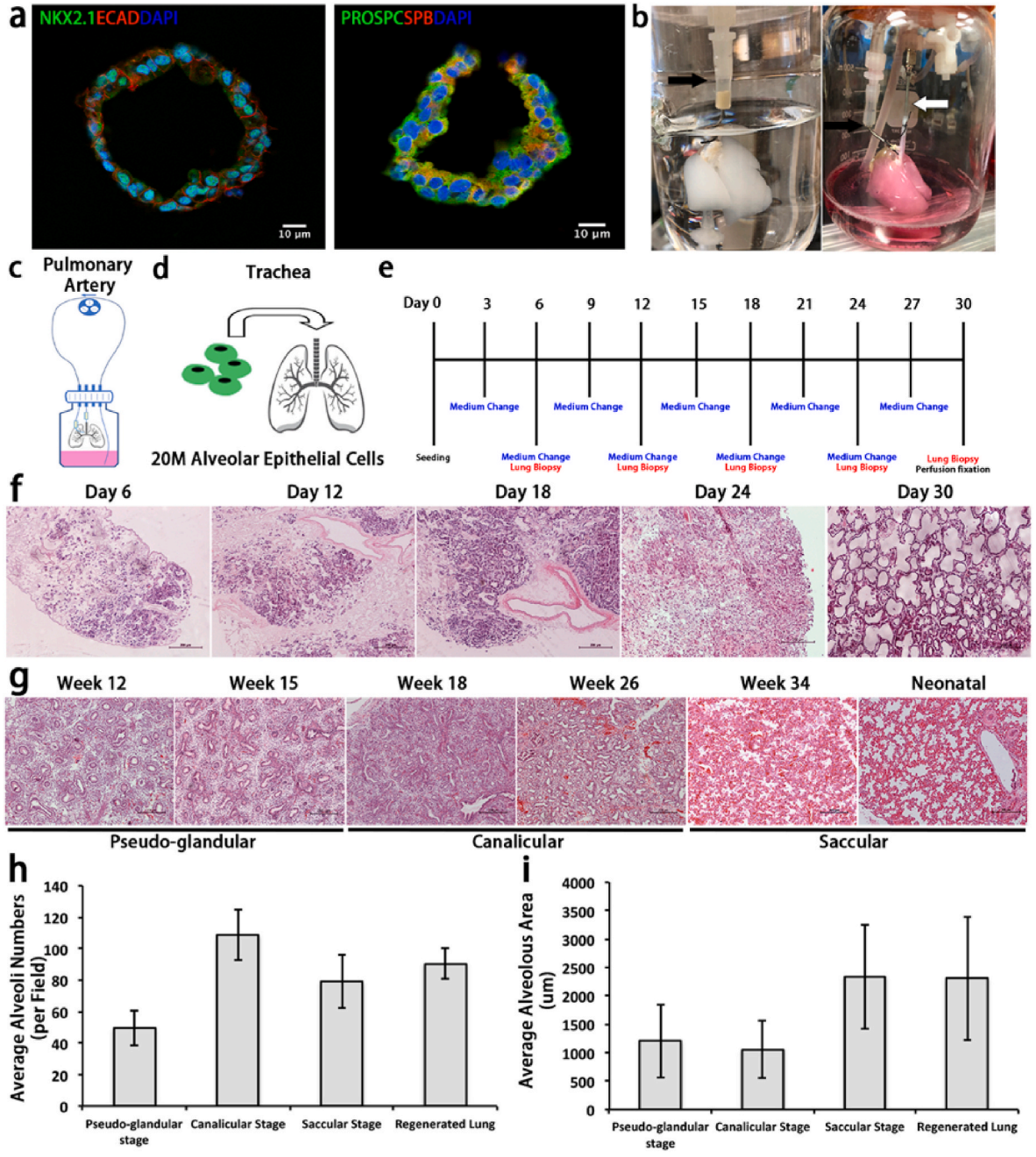

Fig. 1. Recellularization and extended organ culture of EMLs. a. Immunofluorescent images of alveolar spheres show the expression of lung epithelial marker protein Nkx2.1 and CDH1, AT2 marker protein ProSPC and SPB. Scale bar = 10 μm. **b.** Rat lung decellularization chamber and bioreactor for extended organ culture. Black arrows point at pulmonary artery (PA) cannulas, white arrow points at trachea cannula. **c.** Schematic of the biomimetic culture system show the bioreactor design and roller pump layout. **d. & e.** Overview of scaffold seeding, culture, medium change and sample collection strategies. The order for lung biopsies are shown in Supplementary Table 1. **f.** Representative H&E images show the structure of cross-sections of engineered rat lungs after 6, 12, 18, 24, and 30 days of extended organ culture. Scale bar = 200 μm. **g.** Representative H&E images showing the structure of fetal human lungs at week 12, 15, 18, 26, 34, and neonatal stages. Scale bar = 200 μm. **h.** Morphometric analysis showing average alveolar number of EMLs at organ culture day 30 and fetal/neonatal human lungs per 700 μm × 252 μm fields (n = 3 individual lungs for each stage). **i.** Comparison of average alveolar size of EMLs at organ culture day 30 and fetal/neonatal human lung (n = 3 individual lungs for each stage). The increase of alveolar number and the decrease of average alveolar area from pseudoglandular to canalicular stages indicated the expansion of distal airways, while the decrease of alveolar number and increase of average alveolar size from canalicular to saccular stage correlated well with the onset of liquid and/or air ventilation during development [57].

exchange tissue containing both AT1 and AT2 cells has not been accomplished to date.

By following existing differentiation protocols with modifications, we generated alveolar spheres from human iPSCs and seeded single alveolar epithelial cells (AECs) onto acellular whole rat lung matrixes, then successfully engineered human distal lung epithelium through extended biomimetic organ culture (extended organ culture). Analysis of the regenerated tissue confirmed extensive re-epithelialization with architecture and morphology like that seen in early-stage lung development. Gene expression analysis showed the presence of AT2 and AT1 phenotypes on engineered lungs.

Our engineered miniature lungs (EML) can be used as a comprehensive SARS-CoV-2 infection and pathogenesis model. However, infecting these engineered organs with the replication competent virus requires access to a biosafety level 3 laboratory. Due to this limitation, we used a Spike protein pseudotyped, single round lentiviral vector to infect our EML. This virus is unable to recapitulate the entire lifecycle of SARS-CoV-2. However, many of the current therapeutic agents (including monoclonal antibodies and neutralizing antibodies stimulated by the vaccines) target the entry step. Therefore, EML infected with Spike pseudotyped virion can be used to examine the entry step of SARS-CoV-2 and evaluate various therapeutic agents that target this critical step of the viral lifecycle. Using this system we confirmed that the viral entry to distal epithelial tissue is ACE2 dependent. We further compared the entry efficiency of the D614G variant of SARS-CoV-2 compared to the original Wuhan strain and examined the ability of two protease inhibitors to block the infection of the engineered epithelium. The present dataset shows that EMLs can bridge the gap from iPSC derived distal lung cells and organoids to more mature distal lung epithelium and provide a physiologically relevant model for the study of the SARS-CoV-2 viral pathobiology and the evaluation of therapeutic interventions.

2. Results

2.1. Characterization of human lung epithelium in engineered miniature lungs

Purified alveolar epithelial cells derived from BU3-NGST cells were embedded in Matrigel drops for expansion. The expression of the epithelial cell marker E-Cadherin (E-Cad, CDH1), the lung progenitor marker NKX2.1, and the AT2 cell markers Pro-SPC and surfactant protein B (SPB) were confirmed by immunofluorescent staining (Fig. 1a), indicating that AECs generated from human iPSCs indeed exhibited features of AT2 cell identity *in vitro*. In preparation for cell seeding, acellular rat lungs were cannulated via trachea and pulmonary artery (PA), enabling cell seeding via airway and constant media perfusion via the pulmonary vasculature (Fig. 1b&c). Rat lungs were each seeded with 20 million AECs and were maintained in extended organ culture for 30 days (Fig. 1d&e). One lobe of each regenerated lung was removed every 6 days for analysis (Supplementary Table 1). We observed increasing epithelial coverage over the culture duration, suggesting continuous proliferation of AECs on scaffolds (Fig. 1f, Supplementary Fig.1a). Histologic analysis of the engineered lung at later stages of culture, such as 24 and 30 days, revealed an increasingly organized distal lung epithelium (Fig. 1f). To better understand the level of maturity and to match engineered lungs with human developmental stages, we obtained fetal and neonatal human lungs from pseudoglandular, canalicular and saccular stages. We observed comparable morphology of engineered lungs at culture day 30 to late canalicular to early saccular stage human lung tissue (Fig. 1g), showing the formation of distal airway and the completion of branching morphogenesis [20, 21]. Histologic analysis of fetal/neonatal rat lung supported a similar conclusion (Supplementary Fig.1b). We then calculated the average area and number of alveoli in fetal/neonatal human lungs and engineered lung at 30 days of extended organ culture. Via morphometric analysis, we observed that alveolar size in engineered lungs gradually increased over the culture duration, ultimately reaching metrics comparable to fetal/neonatal human lung at late canalicular to early saccular stages (Fig. 1 h&i). Immunofluorescent staining of engineered lungs showed the persistent expression of Nkx2.1, CDH1, ProSPC, and SPB throughout organ culture (Fig. 2a&b). Compared to *in vitro* cultured AECs, engineered lung tissue showed a higher expression of CDH1 throughout the culture duration, and initially equivalent levels of Nkx2.1, which decreased towards to end of culture (Fig. 2c). The expression of ProSPC was slightly lower in engineered tissue, while SPB was comparable to AECs. As a point of reference, we analyzed expression of Nkx2.1, CDH1, ProSPC, and SPB in fetal/neonatal lungs at different developmental stages (Fig. 2d&e). The observed gene expression pattern of developing alveoli further indicated that regenerated lungs resemble canalicular stage human lungs to a certain extent.

2.2. Engraftment and proliferation dynamics of AECs in engineered miniature lungs

After an initial engraftment period, we observed stable AEC proliferation over the culture duration with an increase of Ki67 expression from day 6 to day 18 and 24, and a slight decrease at day 30 (Fig. 3a and b). QRT-PCR confirmed that the expression levels of Ki67 were lower at day 6 and day 30, the beginning and end of organ culture, than day 12, 18, and 24 (Fig. 3c). TUNEL staining of lung samples showed consistently low number of apoptotic cells (<10%) throughout the culture duration (Supplementary Fig.1c). These results demonstrated the compatibility of acellular scaffolds and AECs, and a stable cellular proliferation of AECs after engraftment. Corresponding to cell proliferation, we observed a steady increase of epithelial coverage over the culture duration, which ultimately reached 82.04% ± 8.89% at day 30 (Fig. 3d). To correlate morphologic data with viable cell quantification, we performed a Resazurin based metabolic assay before each biopsy [22]. At 6 days after seeding of 20 M cells, 32.88 ± 7.61 M viable cells were found in engineered lungs, and the number reached 99.89 ± 3.14 M by the end of 30 days extended organ culture (Fig. 3e). Glucose consumption and lactate production in culture medium both confirmed the continuous proliferation of metabolically active AECs in EMLs (Fig. 3f&g). The levels of pH, pO_2, and pCO_2 remained within healthy limits, but showed a slight trend towards under-perfusion towards the end of culture (Supplementary Fig.1e).

2.3. Emergence of AT1 cells during epithelial maturation

AT2 cells are the progenitor cells of AT1 cells in fetal lung development and homeostasis [23, 24]. After engraftment of a pure AT2 cell population, we observed emergence of Aquaporin 5 (AQP5) expressing cells, the majority of which had no SPB expression, while some showed co-expression of both markers (Fig. 4a). The number of AQP5 expressing cells increased while their morphology changed from cuboidal to squamous over the course of the culture duration (Fig. 4a). This may indicate that *trans*-differentiation of AT2 cells towards an AT1 fate may have occurred. We further observed expression of the human AT2 cell marker protein HTII-280 in a minority of cells at later organ culture days with an average of 0.030% ± 0.012% (Fig. 4b). A similar shift in number and phenotype of AQP5, and HTII-280 positive cells was observed in fetal and neonatal human lungs further supporting the engineered lung's resemblance to canalicular to saccular stage human lungs (Fig. 4c and Supplementary Fig. 2a and b). 3D reconstructions of tissue after 30 days of culture show that engineered epithelium consisted of well-organized, intact alveoli with broad expression of SPB, and luminal expression of AQP5 suggesting a mixed AT1 and AT2 phenotyped epithelium in EMLs (Fig. 4d).

To quantify cell fate conversion during tissue formation, we recorded the number of cells that were expressing only AQP5, SPB, or co-expressing both markers in engineered miniature lungs over time. As shown in Fig. 4e, the ratio of AQP5 expressing cells increased from day 6

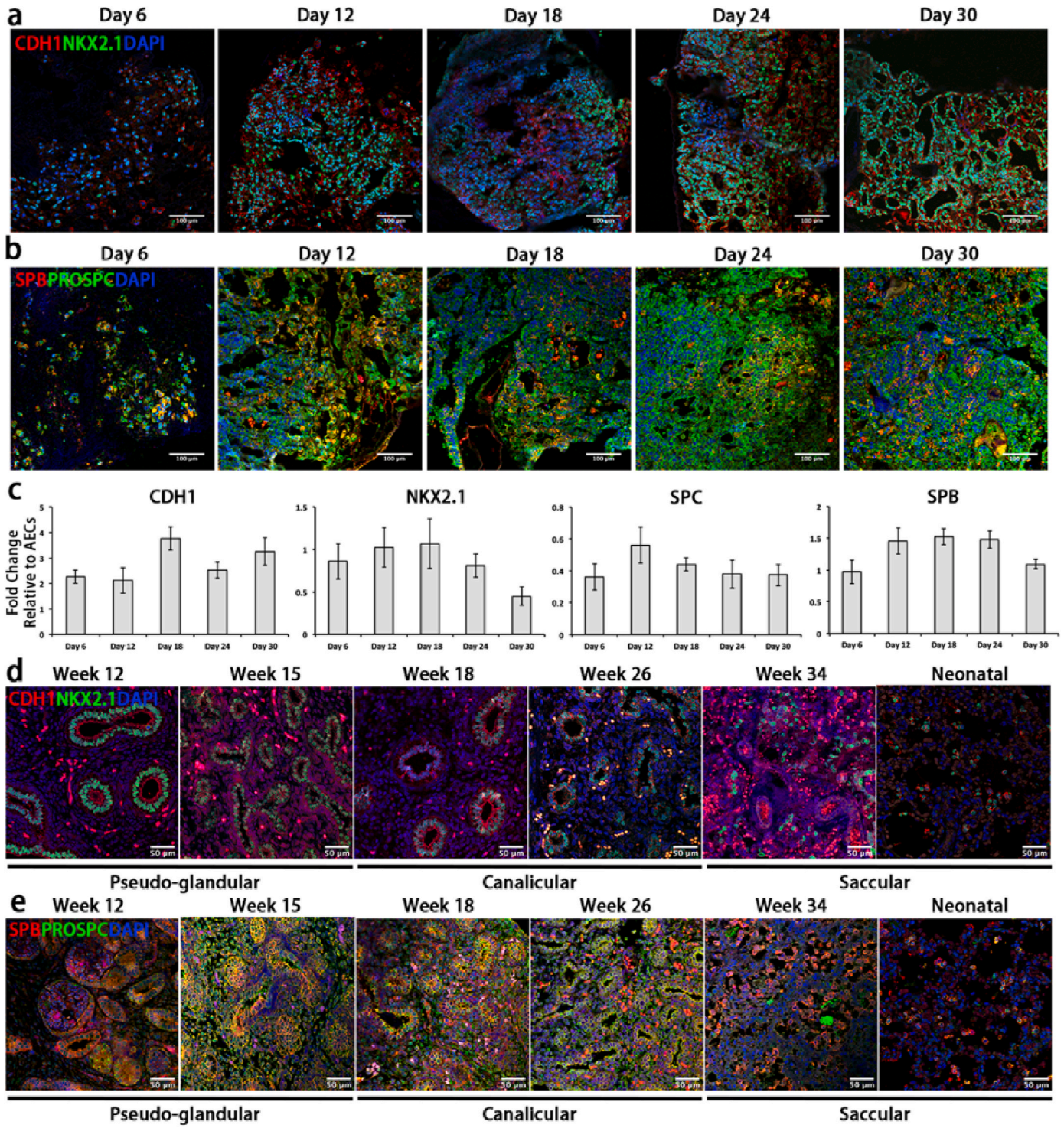

Fig. 2. Phenotypic Characterization of EML tissue. A. Immunofluorescent images show the stable expression of Nkx2.1 and CDH1 in EMLs throughout extended organ culture. Scale bar = 100 μm. **b.** Immunofluorescent staining showing the stable expression of ProSPC and SPB in EMLs through extended organ culture. Scale bar = 100 μm. **c.** Quantitative RT-PCR gene expression analysis of Nkx2.1, CDH1, ProSPC, and SPB in EMLs through extended organ culture. Gene expression levels were normalized to the housekeeping gene beta-actin, and presented relative to *in vitro* cultured AECs. **c.** Immunofluorescent images showing the expression of Nkx2.1 and CDH1 in fetal/neonatal human lungs at different developmental stages. Scale bar = 100 μm. The expressions of lung progenitor marker Nkx2.1 was higher in earlier than later stages. **e.** Immunofluorescent images showing the expression of SPB and ProSPC in fetal/neonatal human lungs at different developmental stages. Scale bar = 100 μm.

to day 24, while the ratio of SPB expressing cells and double positive (DP) cells remained stable during culture. Measurement of fluorescence intensity showed that while the epithelial coverage rate increased constantly during culture, the fluorescent area of SPB and AQP5 had also increased (Fig. 4f). The mean fluorescent intensity of SPB decreased slightly during culture, while AQP5 remained stable (Supplementary Fig.1g). We correlated fluorescent area with mean fluorescent intensity to calculate the integrated density, which showed increase of both SPB and AQP5 in engineered tissue during organ culture (Fig. 4f and g). QRT-PCR results further suggested the appearance of AT1 phenotyped cells

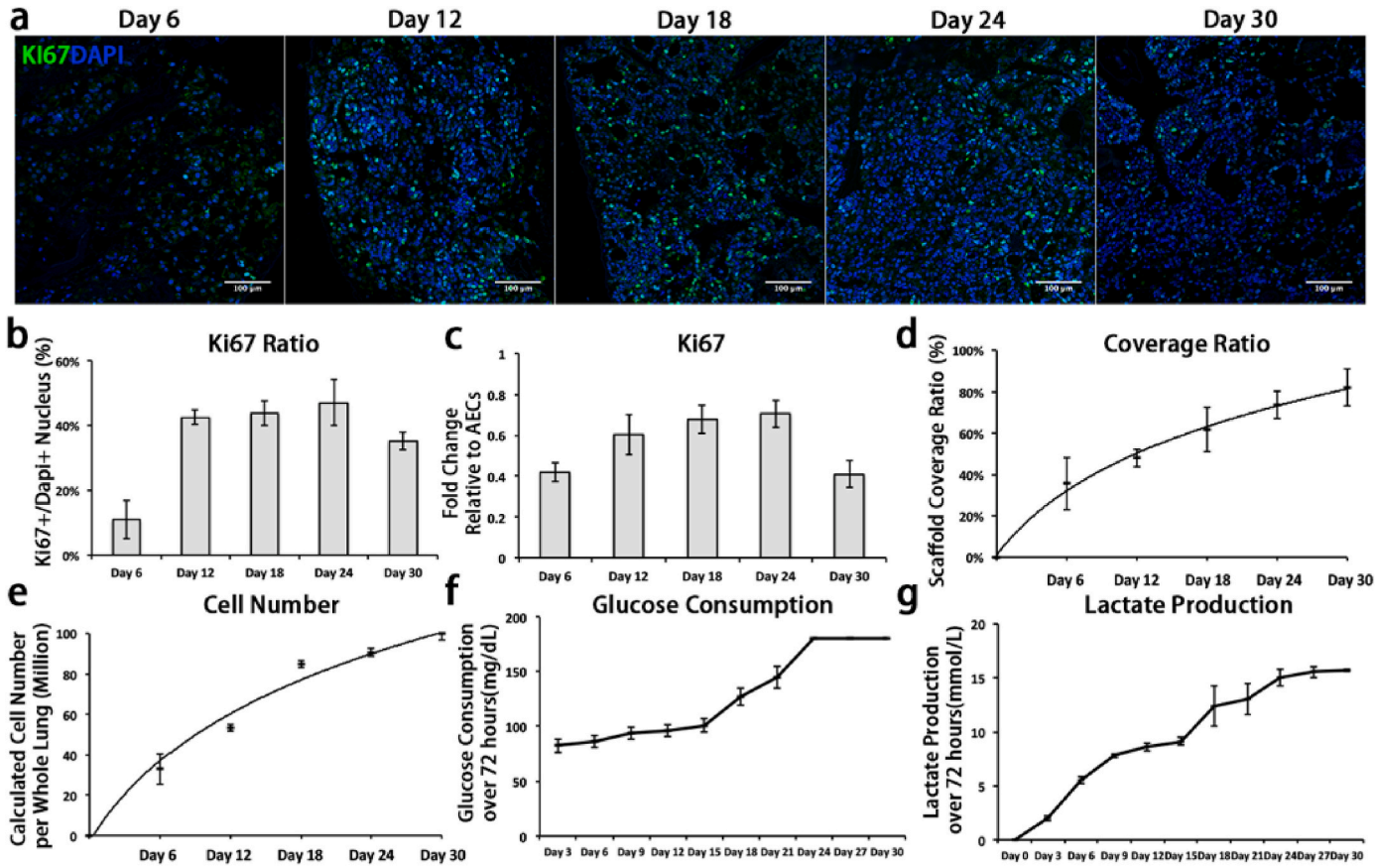

Fig. 3. Engraftment and proliferation dynamics of AECs in EMLs. a. Immunofluorescent staining of Ki67 in EMLs at different organ culture days. Scale bar = 100 μm. **b.** Histogram showing the ratio of Ki67 positive cells over all DAPI positive cells in EMLs at different organ culture days. **c.** Quantitative RT-PCR gene expression analysis of Ki67 in EMLs at different organ culture days showing a similar pattern as immunostaining. Gene expression was normalized to the housekeeping gene beta-actin, levels are shown relative to *in vitro* cultured AECs. **d.** Scaffold coverage calculated by Fiji with H&E images of engineered lung at different organ culture days (n = 4 individual lungs). **E.** Viable cell number estimated by a Resazurin based metabolic assay of EMLs at different organ culture days. The overall number of cells decreased due to the reduction of total lung volume caused by lobe removal, which was measured by average weight of cadaveric rat lungs (Supplementary Fig. 2). To correct for this, cell numbers estimated by Resazurin assay were normalized to the remaining volume of EMLs at the time each essay was conducted (Supplementary Table 1). **f.** Glucose consumption over 72 h of EMLs at different organ culture days. **G.** Lactate production over 72 h of EMLs at different organ culture days. Although the volume of culture medium increased according to the presumed outgrowth of cells during organ culture (Supplementary Table 2), glucose consumption and lactate production still plateaued during later time points (Fig. 3f&g), implying the need for more medium and/or more frequent medium change.

upon extended organ culture by showing that several AT1 markers, including AQP5, Podoplanin (PDPN), and HOPX, all significantly increased during organ culture (Fig. 4e).

2.4. Protease inhibition of SARS-CoV-2 viral entry

To test the validity of engineered miniature lungs as a discovery tool in COVID-19 related research, we studied the viral entry of SARS-CoV-2 in 3D culture and its inhibition with protease inhibitors. SARS-CoV-2 viral entry into lung epithelial cells depends on the cell surface receptor angiotensin-converting enzyme 2 (ACE2) [3]. As a first step, we confirmed ACE2 expression in BU3-NGST alveolar spheres and engineered lung at day 30 of extended organ culture (Supplementary Fig. 3a). We then generated a Spike protein pseudotyped GFP-expressing lentivirus to mimic the viral entry process. To avoid the conflict of Nkx2.1-GFP marker protein expression with GFP expressing pseudotyped virus, we derived a second AEC line from human iPSC SPC2 for the following experiments. SPC2 alveolar spheres showed comparable gene expression levels of ACE2 and TMPRSS2, a protease essential for Spike protein priming, and showed expression of AT2 cell marker genes (Supplementary Fig. 2b and c). We therefore proceeded to seed whole rat lung scaffolds with SPC2 AECs as described and cultured the resulting constructs for 26 days at which point viral infection was induced via tracheal instillation (Fig. 5a&b). H&E staining showed epithelial tissue morphology before and after virus infection as described above (Supplementary Fig.2d). Immunofluorescent staining of GFP and ACE2 in regenerated lung showed that the majority of GFP and ACE2 expression was co-localized, while GFP signals could be observed in live cultured lungs (Fig. 5c&d). A concerning feature of SARS-CoV-2 is its ability to mutate. These viral variants could pose a challenge towards development of effective therapeutic agents. An early amino acid change in the Spike protein of some strains of SARS-CoV-2 was identified early in the pandemic. This variant, labeled D614G has become the dominant form globally since March 31, 2020. *In vitro* experiments have shown that this mutation confers an evolutionary advantage to the virus by increasing viral entry [25, 26]. In our model of engineered miniature lungs, we studied if the D614G mutation alters the entry efficiency of the SARS-CoV-2 [25, 26], and if the infection could be blocked by known protease inhibitors [3, 4]. We cultured EMLs for 24 h with or without 50 μM Camostat Mesyalte at a concentration found to be effective on 2D cultured AECs (Supplementary Fig. 3a, b, d). We then infected EMLs with either wildtype (WT) or D614G viruses while keeping Camostat Mesyalte in culture medium (Fig. 5e). Immunostaining showed that although the expression of cellular receptor ACE2 remained the same across EMLs, pre-treatment with Camostat Mesyalte significantly blocked the viral entry in both WT and D614G virus-infected lungs

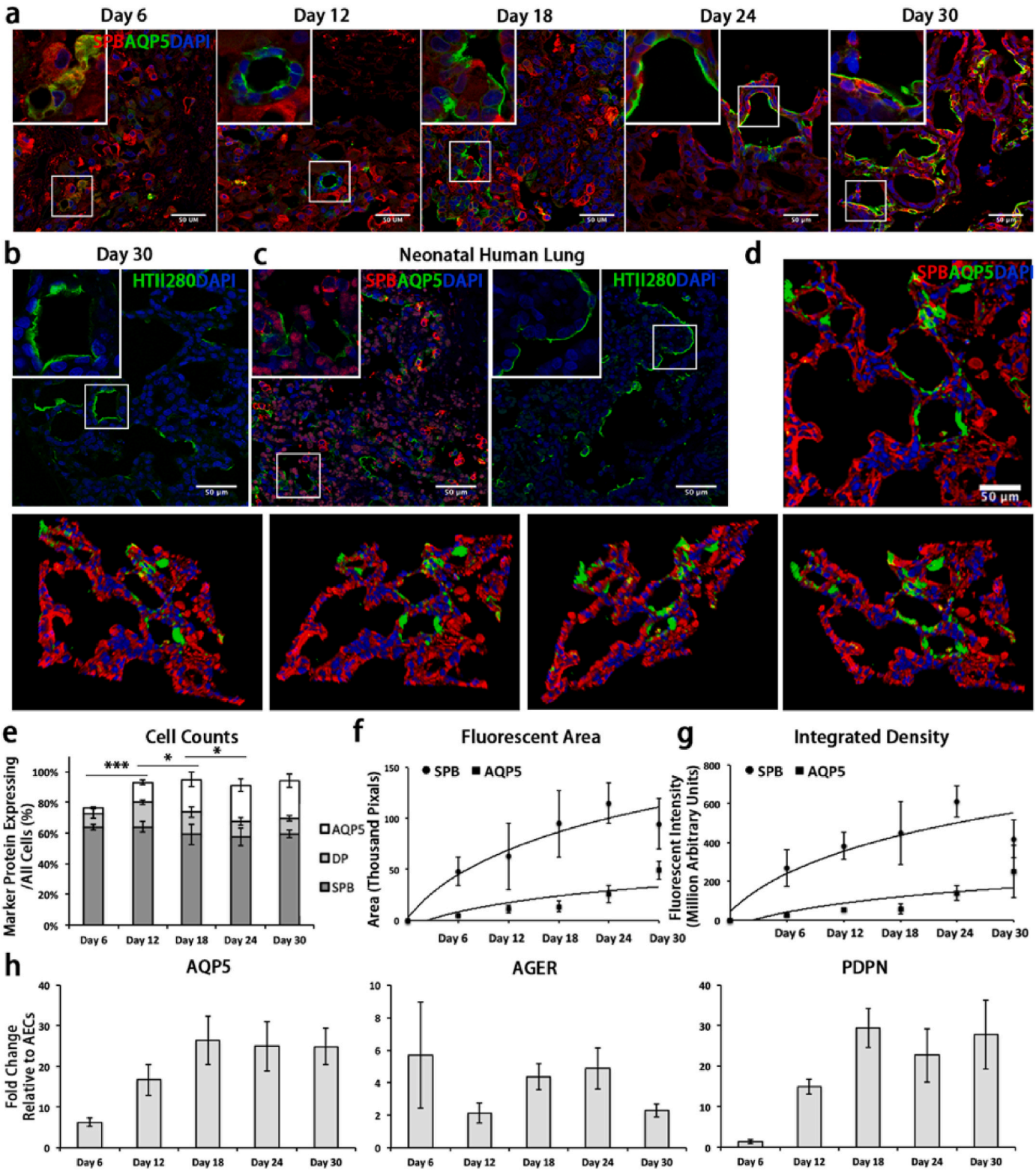

Fig. 4. Emergence of AT1 cells during EML maturation. a. Immunofluorescent staining of EMLs showing the expression of SPB and AQP5 at different organ culture days. Scale bar = 50 μm. **b.** Immunofluorescent staining of EMLs showing the expression of HTII-280 at organ culture day 30. Scale bar = 50 μm. **c.** Immunofluorescent staining showing the expression of SPB AQP5, and HTII-280 in neonatal human lung. Scale bar = 50 μm. The AT1 and AT2 marker expression pattern in EMLs at organ culture day 30 resembles neonatal human lung. Scale bar = 50 μm. **c.** Reconstructed Z-stacks of EMLs at organ culture day 30 generating 3D views of alveoli. **e.** Histogram showing the ratio of AQP5 expressing, SPB expressing, and double positive cells in EMLs at different organ culture days. **f.** Measurement of fluorescent area of SPB and AQP5 in immunofluorescent images of EMLs at different organ culture days. The ratio of AQP5 expressing cells increased significantly from day 6 to day 24. **g.** Calculation of integrated densities of SPB and AQP5 of immunofluorescent images of EMLs at different organ culture days. **h.** Quantitative RT-PCR gene expression analysis of AQP5, AGER, and PDPN in EMLs at different organ culture days. Gene expression levels were normalized to the housekeeping gene beta-actin, and presented relative to *in vitro* cultured AECs.

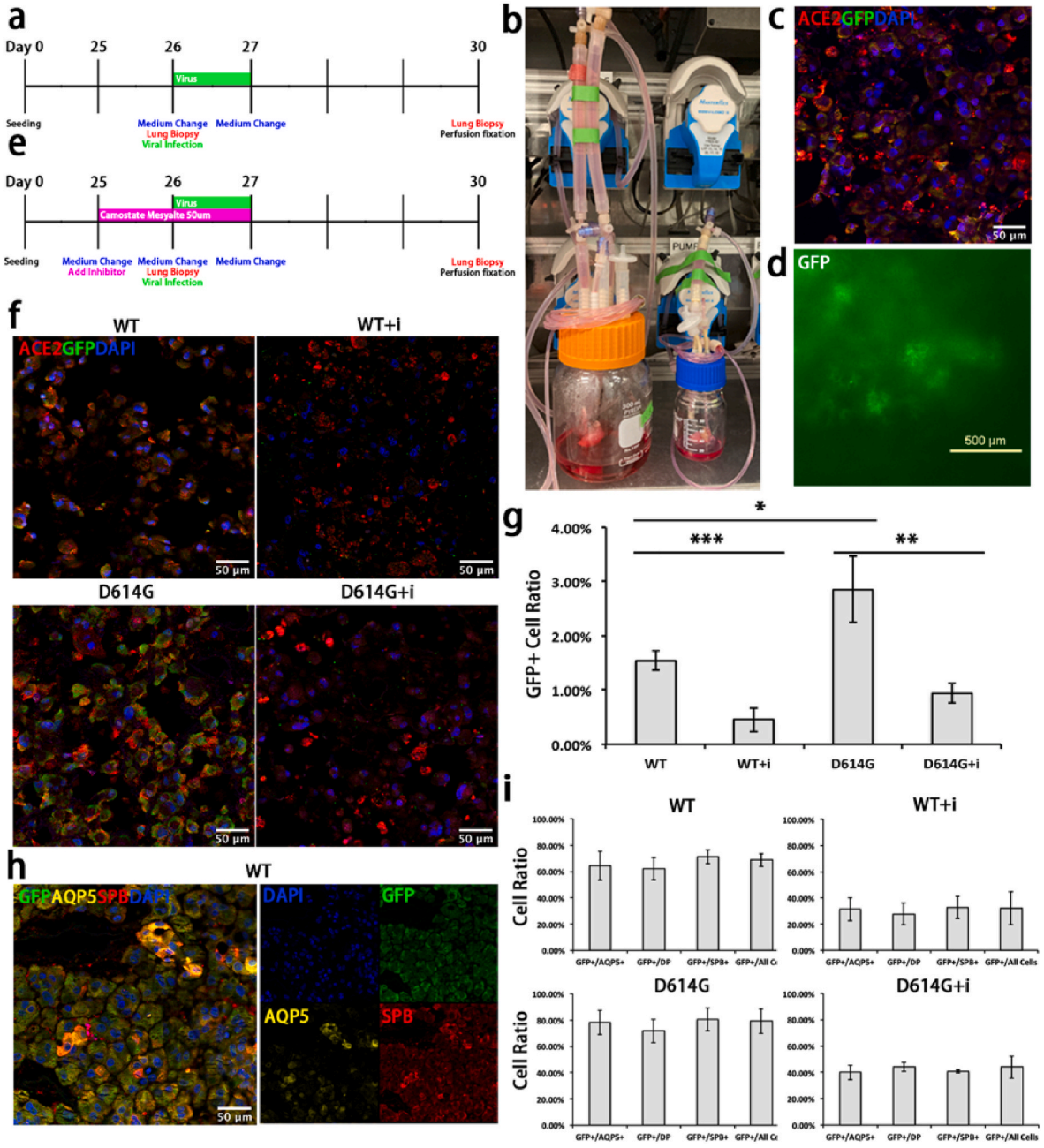

Fig. 5. Modeling of SARS-CoV-2 viral entry and protease inhibition with pseudotyped lentiviruses. a. Timeline of viral infection experiments in EMLs (rat lung seeding, culture, viral infection and sample collection). **b.** Rat lung bioreactors for routine extended organ culture (Left) and viral infection (Right). We designed a small sized organ culture bioreactor system that allowed us to use as few as 25 mL of virus containing medium for the system. **c.** Immunofluorescent images show the expression of ACE2 and GFP in EMLs 3 days after WT viral infection. Scale bar = 50 μm. **d.** Live image of engineered EML 3 days after viral infection showing the expression of GFP in infected cells. Scale bar = 500 μm. **e.** Timeline of virus variant and protease inhibition experiments in EMLs (rat lung seeding, culture, protease inhibitor application, viral infection and sample collection). **f.** Immunofluorescent images showing expression of GFP and ACE2 in EMLs 3 days after WT or D614G viral infection, with or without 50 μM Camostat Mesylate. Scale bar = 50 μm **g.** Flow cytometry analysis of GFP + cells in EMLs 3 days after WT or D614G viral infection, with or without 50 μM Camostat Mesylate pretreatment. **h.** Immunofluorescent images showing the expression of GFP, AQP5, and SPB in EMLs 3 days after WT viral infection. Scale bar = 50 μm for merged image. **i.** Histograms show the ratio of GFP + cells amongst AQP5 expressing cells (GFP+/AQP5+), SPB expressing cells (GFP+/SPB+), double positive cells (GFP+/DP), and all cells (GFP+/All cells) in EMLs 3 days after WT and D614G virus infection, with or without 50 μM Camostat Mesylate pretreatment.

(Fig. 5f). As expected, non-treated D614G virus infected lungs overall showed more GFP + cells than non-treated WT virus infected lungs (Fig. 5f). The infection of pseudotyped viruses and the addition of Camostat Mesyalte did not change the identities of AECs on engineered lungs as shown by the immunostaining of AEC marker proteins (Supplementary Fig.3c). Flow cytometry analysis of GFP + cells in single cells isolated from regenerated lungs further proved this conclusion (Fig. 5g, Supplementary Fig.3e). By testing different exposure and incubation times of Camostat Mesyalte on both 2D cultured AECs and EMLs, we had confirmed that pre-treatment of this small molecule together with co-incubation during viral infection inhibited viral entry most significantly (Supplementary Fig. 3e and f). At last, we analyzed if the entry of pseudotyped viruses in EMLs was restricted to epithelial cells of a certain phenotype. Immunostaining showed that GFP signal

could be detected in both AQP5 expressing, and SPB expressing epithelial cells, indicating that AECs exhibiting AT1, AT2, or intermediate phenotypes were susceptible to infection by both pseudotyped viruses, either WT or D614G (Fig. 5h, Supplementary Fig.4a). We quantified the ratio of GFP expression in AQP+, SPB+, DP, and all cells, the result showed no significant differences of viral infection efficiency between different cell populations (Fig. 5i). In all engineered lungs infected by either WT or D614G, with or without Camostat Mesyalte, we observed ACE2 expression among all cell populations as well, indicating the SARS-CoV-2 pseudotyped viral infection was mediated by ACE2 in AECs with AT1 phenotype as well as AT2 phenotype (Supplementary Fig.4b).

3. Discussion

The worldwide COVID-19 pandemic has cost over 6 million lives and continues to challenge health care systems and humanity across the globe. While various vaccines have shown drastic effects on preventing COVID-19 infection and reducing its severity, the discovery of effective novel forms of treatment of COVID-19 has lagged behind. To study this devastating disease and its pathophysiology, *in vitro* models mimicking human lung tissue including 3D cultured organoids [5–8], air-liquid interface cultured epithelium [11, 27–29], and lung-on-a-chip models [9–13] have provided valuable research platforms. However, none of these replicate the structure of human lungs, therefore limiting the ability to simulate and analyze critical events during and after COVID-19 infection, including the primary infection, disease progression and the related pathophysiology of airway cells [30]. We have learned that the Spike protein of SARS-CoV-2 mediates binding to ACE2 to enter target cells. ACE2 is an important regulator in the renin-angiotensin-system (RAS) and plays crucial role in SARS-CoV induced lung injury [31, 32]. Similarly, SARS-CoV-19 uses ACE2 as a receptor for cellular entry [33, 34], the expression of which had been found in lung AT2 cells [35]. Autopsy samples showed that diffuse alveolar damage was found in many severe COVID-19 patients, while pulmonary alveolar regeneration led by AT2 cells was observed in some survivors [1, 2, 36]. Currently available 2D and 3D models built on primary or iPSC derived cells have not reached functional maturity of a mixed AT1/AT2 cell epithelium and therefore cannot simulate epithelial infection, damage, and repair.

Over the past decade, several groups have developed and refined organ engineering techniques based on perfusion decellularized lung scaffolds [37]. While engraftment of epithelial cells has been described, to date no mature epithelial phenotype and morphology has been detected in engineered tissue constructs [38, 39]. Recently, improved differentiation efficiency of lung epithelial cells derived from human iPSCs has been described, yet extensive distal lung tissue formation and surfactant secretion has yet to be obtained [40].

In the present study we aimed to show that iPSC derived AECs can be engrafted on rat lung scaffolds to form engineered miniature lungs. When cultured over extended time, iPSC derived AECs mature formed a stage corresponding to the pseudoglandular stage [41] featuring an epithelium corresponding to late canalicular to early saccular stage with a gradually increasing number of AQ5 expressing AT1 phenotyped cells and HTII-280 expressing AT2 cells. Aquaporin 5 expression identifies AT1 cell fate [42], yet additional work is required to fully understand this emerging cell type during tissue formation in EMLs. To date, no *in vitro* differentiation protocol for the generation of AT1 cells from human iPSCs has been reported. Our results indicate that the process of tissue formation on acellular scaffolds may contribute signals that drive cell fate conversion from an AT2 to an AT1 phenotype. HTII-280 had been found to be a human AT2 cells specific surface marker protein [43], and had been widely used for purification of primary AT2 cells from donor human lungs [19, 44, 45]. It is developmentally regulated, and the expression level increases with gestation weeks [43]. The expression of HTII-280 has not been described in human iPSC derived alveolar spheres [18, 19, 46]. Our data further showed the expression of ACE2 in a large number of isolated AECs, and confirmed that Spike protein mediated viral entry is ACE2 dependent in both isolated AECs and EMLs.

The emergence of SARS-CoV-2 variants worldwide may affect the clinical impact on patients and the efficiency of vaccines developed to date [47]. To examine the usefulness of our model in studying this shift, we tested if the infection efficiency would be noticeably impacted by a known more contagious variant. The D614G variant significantly increased the efficiency of viral entry in both AECs cultured in spheres and EMLs, in line with previous *in vitro* and *in vivo* observation [25, 26]. We further examined whether the infection could be blocked by three reported protease inhibitors that had been shown to block ACE2 dependent SARS-CoV-2 virus entry [3, 4]. Camostat Mesyalte pre-treatment indeed blocked viral entry in cultured SPC2 AECs while E64-D and Apilimod had a much more subtle effect. The Cathepsin L inhibitor E64-D has been reported to have a significant role inhibiting SARS-CoV-2 infection [3, 48], while Apilimod as a PIKfyve kinase inhibitor has been shown to antagonize both virus entry and replication [4, 49]. This discrepancy may be related to cell line specific differences and may indicate the role of alternative ACE2 independent infection mechanisms. To reduce the necessary biosafety level, we chose to utilize a pseudotyped lentivirus to study viral entry as the very first step of virus infection. In our study, virus was applied through trachea to resemble the primary route of infection in COVID-19 patients, while the inhibitor was added to the culture medium and delivered to the whole lung through pulmonary perfusion. After infection, we analyzed the ratio of infected GFP + cells in AECs exhibiting AT1, AT2, and AT1/2 phenotypes. We observed no significant differences of viral infection amongst the various populations, while we detected ACE2 expression in all cell types. SARS-CoV-2 infection in AT1 cells as well as AT2 and intermediate cells had been reported in patients who succumbed to COVID-19 [17], which is in line with our finding on EMLs. The expression of ACE2, the mediator of SARS-CoV-2 virus, in AT1 cells is somewhat controversial as recently shown by recent reports of single cell RNA sequencing projects of human lungs [15, 50]. Additionally, ACE2 expression was found by immune staining in both AT1 and AT2 cells [51]. Our study confirmed ACE2 expression in human iPSCs derived AT1 phenotyped cells. These could further be infected by pseudotyped SARS-COV-2 virus, indicating the entry of SARS-CoV-2 in AT1 cells may be mediated by ACE2 similar as in AT2 cells.

In summary, human EMLs represent a novel small-scale model of human lungs enabling the study of viral infection and evaluation of novel treatment options *in vitro*. The use of fully competent virus and a fully endothelialized system may further enable examination of physiologic effects of viral infection and tissue repair and recovery.

4. Methods

4.1. Study approval

All experiments were approved by Massachusetts General Hospital (MGH) Animal Utilization Protocol #2014N000261. Cadaveric human lung was obtained through International Institute for the Advancement of Medicine (IIAM) under an approved protocol named 'NEONATE En Bloc or Individual Lung'. Fixed fetal human lung samples were obtained through MGH Department of Pathology and approved by Human Material Excess Protocol #2020P000560.

4.2. Plasmids and viral constructs

The psPAX2 plasmid was a gift from Didier Trono (Addgene plasmid # 12,260; http://n2t.net/addgene:12260; RRID:Addgene_12,260) and is a lentiviral packaging vector. The pSin-GFP-IRES-Puro vector was made using pSin-EF-Sox2-Puro, which was a gift from James Thomson (Addgene plasmid # 16,577; http://n2t.net/addgene:16577; RRID: Addgene_16,577). The gfp ORFs was subcloned into the pSin-EPB-IRES-Puro using the *Eco*RI and *Bam*HI sites.

The vectors expressing the Spike proteins are a modification of a PiggyBac (PB) vector generously provided by Sahand Hormoz. The codon-optimized spike gene was PCR-amplified from a plasmid obtained from Sino Biological (VG40589-UT). This amplicon was further modified to lack the C-terminal 19 amino acids and instead contains a C-terminal HA tag (YPYDVPDYA). We used the NEBuilder® HiFi DNA Assembly Cloning Kit from the New England Biolabs for cloning the S-D614-ΔC-HA amplicon into the PB vector. The PB-S-G614-ΔC-HA vector is obtained from the PB-S-D614-ΔC-HA vector using the Quickchange XL Site-directed Mutagenesis (Agilent).

4.3. Pseudotyped virus production and quantification

HEK293T cells were seeded in T150 flasks at ~50% confluency one night prior to the transfection. The next day, the cells were co-transfected with pSin-GFP-IRES-Puro, the psPAX2 packaging vector, and the Spike-expressing PB plasmid (S-D614-ΔC-HA or S-G614-ΔC-HA) at 1:1:1 M ratio for a total DNA concentration of 40 μg was used to transfect the cells using the TransIT®-LT1 Transfection Reagent (Mirus Bio). Three days later, the supernatant was collected and spun at 350×*g* for 10 min at 4 °C, then filtered through a 0.45 μM filter. The virus was then pelleted by ultracentrifugation at 100,000×*g* over a 20% sucrose cushion. The virus was then quantified using the Lenti-X™ p24 Rapid Titer Kit (Takara Bio) and aliquots were frozen at −80 °C for future use.

4.4. Generation of alveolar spheres from human iPSCs

The differentiation of iPSCs was performed following previously published protocols with modifications [18, 19, 41, 52, 53]. Briefly, BU3-NGST iPSC that carries two fluorescent reporters, Nkx2.1^{GFP} and SPC^{tdTomato}, and SPC2 iPSC that carries fluorescent reporters SPC^{tdTomato} were maintained in mTeSR medium (Stemcell Technology) and started to undergo differentiation when cells reached 60–70% confluence, with a step-wised procedure that mimics lung developmental stages [1]: Definitive endoderm: StemDiff definitive endoderm kit (Stemcell Technology), 4 days [2]. Anteriorized endoderm: 1 μM A8301 (Sigma), 1 μM IWR-1 (Tocris), 4 days [3]. Ventralized endoderm: 10 ng/mL FGF-7 (Peprotech), 10 ng/mL FGF-10 (Peprotech), 10 ng/mL BMP4 (Peprotech), 3 μM CHIR99021 (Tocris), 100 nM Retionic Acid (Sigma), 7 days. The basal medium for all differentiation steps was DMEM/F12 supplemented with B-27. After ventralization, BU3-NGST cells were stained with DAPI (Sigma) for flow cytometry purification of GFP + cells, and SPC2 cells were stained with DAPI, CD47 (323,108, Biolegend), and CD26 (302,704, Biolegend) for flow cytometry purification of CD47^{high}CD26^{low} cells. Sorted cells were embedded in 100% Growth factor reduced Matrigel (Corning) drops for the formation of alveolar spheres. The culture medium for the formation and maintenance of alveolar spheres was: 50% Medium 199 (Life Technologies), 50% DMEM/F12 (Life Technologies), 2% FBS (Hyclone), B-27 (Life Technologies), 10 ng/mL FGF-7, 10 ng/mL FGF-10, 3 μM CHIR99021, 0.1 mM IBMX (Sigma), 0.1 mM 8-Bromo-cAMP (Sigma), 50 nM Dexamethasone (Sigma), 10 μM Y-27632 (Cayman Chemical), and 50 μg/mL Ascorbic Acid (Stemcell Technology).

After 1–2 weeks of culture for the sorted cells, Matrigel drops were digested by Dispase (Corning) and spheres were trypsinized for purification of GFP+/TdTomato + cells from BU3-NGST cells or TdTomato + cells from SPC2 cells by flow cytometry. Purified cells were seeded at 2 × 10^4 per 100 μl Matrigel in each drop on 12 well plate and cultured in the medium described above.

4.5. Lung decellularization

Cadaveric rat lungs were decellularized as previously described [37, 54, 55]. Rat lungs were explanted from male Sprague-Dawley rats (250–300 g, Charles River Laboratories) and pulmonary artery (PA) of each lung was cannulated. Lungs were then perfused by 0.1% sodium dodecyl sulfate (SDS) solution through PA for 2 h, followed by 15 min of deionized water, 10 min of 1% Triton X-100, and extensive PBS washing in decellularization chamber.

4.6. Seeding of AECs on rat acellular scaffold and biomimetic culture of regenerated lungs

Rat lungs were mounted in bioreactors prefilled with 100 mL alveolar sphere expansion medium then perfused for 1 h by PA at 1 mL/min, in a 37 °C, 5% CO_2 incubator, where the remainder of culture were carried out. Alveolar spheres were trypsinized into single cells and 20 million alveolar epithelial cells re-suspended in 50 mL medium obtained from the bioreactors were seeded into each lung and delivered via airways by gravity at a height of 30 cm.

After seeding, the bioreactors were returned to incubator and given a 1.5–2 h static culture time for cell attachment. PA perfusion was then reinitiated at 4 mL/min and carried on through the culture. Culture medium was changed every 3 days with increased volume every 2 changes, while one lobe was removed for biopsy every 6 days (Fig. 1f, Supplementary Table 1). RNA samples were stored in Trizol (Life Technologies) and rest of the lung was fixed with 4% Paraformaldehyde (PFA) overnight. On day 30, left lung was perfusion fixed through the trachea overnight.

4.7. Pseudotyped virus infection of alveolar epithelial cells and engineered lungs

Alveolar spheres were trypsinized to generate single cells then seeded on 1% Matrigel coated 48 well tissue culture plates for infection. Attached cells were incubated with 100 μl of virus containing medium for 1 day then changed back with alveolar cell medium. For small molecule test, medium containing 20 μM or 50 μM Camostat Mesylate (SigmaAldrich) or E64-D (SigmaAldrich), and 2 μM or 10 μM Ampilimod (MedChemexpress) was added to cells 1 day before infection, and was kept in the medium during infection. Engineered lungs cultured for 26 days were transferred from original incubator for extended organ culture to a new small incubator which runs with a minimum of 25 mL medium (Fig. 5b). Medium containing WT or D614G pseudotyped viruses were added into the incubator and perfused at 1 mL/min for 24 h before transferring back to the normal organ culture incubators. For small molecule inhibition assay on the regenerated lung, medium containing 50 μM Camostat Mesylate was used for lung perfusion starting from Day 25, 24 h before virus infection.

4.8. Resazurin reduction assay on regenerated lungs

Resazurin assay was performed as previously described [22]. Briefly, alveolar spheres were trypsinzed and plated on 1% Matrigel coated 96 well plate with cell/medium ratios of 2, 1, 0.5, 0.25, 0.1, 0.05, 0.025, and 0.01 millions/ml, 100 μl medium per well for standard curve. Triplicate experiments were performed for each dilution. The resazurin-based PrestoBlue cell viability reagent (Life technology) was added to each well at 1:20 (v/v) 6 h after seeding then incubated for 1 h. Fluorescence of medium was read by SpectraMax Microplate Reader (Molecular Devices) at 544 nm (ex)/590 nm (em). For regenerated lungs, the assay was performed every 3 days before medium change. 76 mL of culture medium was kept in each bioreactor with 4 mL of PrestoBlue reagent added. 1 mL of resazurin-medium mixture was saved as non-metabolized control before perfusion. Lungs were then perfused for 1 h and fluorescence of the non-metabolized and metabolized mixture were read. The estimated cell number per whole lung was calculated by standard curve first, then normalized with the remaining lung volume (Supplementary Table 1, Supplementary Fig.1d).

4.9. Histological and immunofluorescent staining

Alveolar spheres were first embedded in Histogel (Thermofisher), then paraffin-embedded and sectioned the same way as PFA-fixed tissue. The sections were stained with Hematoxylin/Eosin for histology, or underwent antigen retrieval and permeabilization with 0.1% Triton-X100 for immune-fluorescent staining. The protocol included blocking by 5% donkey serum (Sigma), incubation with primary antibodies (1:200, Nkx2.1: ab76013, Abcam; E-Cadherin: 610,181, BD Biosciences; Pro-SPC: WRAB-9337, Seven Hills Bioreagents; Surfactant protein B: sc-133,143, Santa Cruz; Aquaporin 5: ab92320, Abcam; Ki67: AB9260, Millipore; AE2, AF933, R&D; GFP, ab6673, Abcam) overnight at 4 °C, washing with PBS for 3 times, incubation with secondary antibodies (1:1000; Alexa Fluor 488 or 546, Life Technologies) for 1 h at room temperature, and mounting with DAPI Fluoromount-G (Fisher Scientific). TUNEL staining was performed following manufacturer's protocol (Promega). Images were captured using Nikon Ti-PFS inverted microscope and Leica SP8 confocal microscope. All the data for quantification of histological and immunofluorescent staining were measured by Fiji.

4.10. Analysis of engineered lung culture medium

Every 3 days, medium was collected before medium change then analyzed with CG4 and G+ cartridges (Abbott) by iSTAT (Abbott).

4.11. Quantitative reverse transcription polymerase chain reaction (RT-PCR)

RNA was isolated by Trizol then reverse transcribed to cDNA by SuperScript Vilo master mix (Life Technologies). Gene expression was quantified by Taqman assay (Life Technologies) using the One Step Plus system (Applied Biosystems). Gene expression was analyzed by normalizing to housekeeping gene beta-actin, and presented relative to *in vitro* cultured alveolar spheres.

4.12. Flow cytometery analysis of GFP + cells in pseudotyped virus infected alveolar epithelial cells and EMLs

Regenerated lungs were digested following a previously published protocols with modifications [56]. Briefly, regenerated lungs were cut into small pieces on ice and about 300 mg tissue was placed in C tubes (Miltenyi) of gentleMACS with 5 mL of digestion buffer consisting of Collagenase I (Life technologies), Dispase (Corning), and DNAse (Roche). Tubes were placed on gentleMACS device and program 'm_lung_01_02' program was run for 2 times. Tubes were then incubated in 37 °C water bath for 30 min. Digested tissue was filtered through 70 μm meshes to generate single cell suspension, then washed twice with PBS. Single cells isolated from regenerated lung and alveolar epithelial cells cultured on tissue culture plate were stained with viability dye 450 (eBiosciences) then fixed with fixation/permeabilization solution kit (BD biosciences). Fixed cells were stained with GFP antibody (ab6673, Abcam) for following analysis on AriaII (BD biosciences).

Declaration of competing interest

The authors declare the following financial interests/personal relationships which may be considered as potential competing interests: Harald C Ott reports financial support was provided by United Therapeutics Corp. H.C.O. is founder and stockholder of IVIVA Medical, Inc. This relationship did not affect the content or conclusions contained in this manuscript. Others declare no competing interests.

Acknowledgements

This work was supported by the United Therapeutics Corporation and by the Charles and Sara Fabrikant MGH Research Scholarship. We thank Dr. Darrell Kotton (Boston University) and Dr. Jessie Huang (Boston University) for providing us BU3-NGST and SPC2 human iPSC lines.

Appendix A. Supplementary data

Supplementary data to this article can be found online at https://doi.org/10.1016/j.biomaterials.2022.121509.

References

[1] K. Wang, et al., Analysis of the clinical characteristics of 77 COVID-19 deaths, Sci. Rep. 10 (2020) 16384.
[2] B.T. Bradley, et al., Histopathology and ultrastructural findings of fatal COVID-19 infections in Washington State: a case series, Lancet 396 (2020) 320–332.
[3] M. Hoffmann, et al., SARS-CoV-2 cell entry depends on ACE2 and TMPRSS2 and is blocked by a clinically proven protease inhibitor, Cell 181 (2020) 271–280 e278.
[4] L. Riva, et al., Discovery of SARS-CoV-2 antiviral drugs through large-scale compound repurposing, Nature 586 (2020) 113–119.
[5] J. Huang, et al., SARS-CoV-2 infection of pluripotent stem cell-derived human lung alveolar type 2 cells elicits a Rapid epithelial-intrinsic inflammatory response, Cell Stem Cell 27 (2020) 962–973 e967.
[6] H. Katsura, et al., Human lung stem cell-based alveolospheres provide insights into SARS-CoV-2-mediated interferon responses and pneumocyte dysfunction, Cell Stem Cell 27 (2020) 890–904 e898.
[7] Y. Han, et al., Identification of SARS-CoV-2 inhibitors using lung and colonic organoids, Nature 589 (2021) 270–275.
[8] T. Wang, et al., Establishment of human distal lung organoids for SARS-CoV-2 infection, Cell Discov 7 (2021) 108.
[9] H.B. Longlong Si, Melissa Rodas, Wuji Cao, , Crystal Yuri Oh, Amanda Jiang, Rasmus Moller, Daisy Hoagland, Kohei Oishi, Horiuchi Shu, Skyler Uhl, Daniel Blanco-Melo, Randy A. Albrecht, Wen-Chun Liu, Tristan Jordan, E. Benjamin, Nilsson-Payant, Logue James, Robert Haupt, Marisa McGrath, Stuart Weston, Atiq Nurani, Seong Min Kim, Danni Y. Zhu, Kambez H. Benam, Girija Goyal, Sarah E. Gilpin, Rachelle Prantil-Baun, Rani K. Powers, Kenneth Carlson, Matthew Frieman, Benjamin R. tenOever, Donald E. Ingber, Human Organ Chip-Enabled Pipeline to Rapidly Repurpose Therapeutics during Viral Pandemics, BioRxiv, 2020.
[10] V.V. Thacker, et al., Rapid endotheliitis and vascular damage characterize SARS-CoV-2 infection in a human lung-on-chip model, EMBO Rep. 22 (2021), e52744.
[11] H. Zarkoob, et al., Modeling SARS-CoV-2 and Influenza Infections and Antiviral Treatments in Human Lung Epithelial Tissue Equivalents, bioRxiv, 2021.
[12] S. Deinhardt-Emmer, et al., SARS-CoV-2 causes severe epithelial inflammation and barrier dysfunction, J. Virol. 95 (10) (2021) e00110–e00121, https://doi.org/10.1128/JVI.00110-21.
[13] A.A. Salahudeen, et al., Progenitor identification and SARS-CoV-2 infection in human distal lung organoids, Nature 588 (2020) 670–675.
[14] H. Zhang, et al., Expression of the SARS-CoV-2 ACE2 receptor in the human airway epithelium, Am. J. Respir. Crit. Care Med. 202 (2020) 219–229.
[15] Y. Zhao, et al., Single-cell RNA expression profiling of ACE2, the receptor of SARS-CoV-2, Am. J. Respir. Crit. Care Med. 202 (2020) 756–759.
[16] L. Guillot, et al., Alveolar epithelial cells: master regulators of lung homeostasis, Int. J. Biochem. Cell Biol. 45 (2013) 2568–2573.
[17] T.M. Delorey, et al., A Single-Cell and Spatial Atlas of Autopsy Tissues Reveals Pathology and Cellular Targets of SARS-CoV-2, bioRxiv, 2021.
[18] K.B. McCauley, et al., Efficient derivation of functional human airway epithelium from pluripotent stem cells via temporal regulation of Wnt signaling, Cell Stem Cell 20 (2017) 844–857 e846.
[19] A. Jacob, et al., Differentiation of human pluripotent stem cells into functional lung alveolar epithelial cells, Cell Stem Cell 21 (2017) 472–488 e410.
[20] K.E. Pinkerton, J.P. Joad, Influence of air pollution on respiratory health during perinatal development, Clin. Exp. Pharmacol. Physiol. 33 (2006) 269–272.
[21] C.R. Rackley, B.R. Stripp, Building and maintaining the epithelium of the lung, J. Clin. Invest. 122 (2012) 2724–2730.
[22] X. Ren, et al., Ex vivo non-invasive assessment of cell viability and proliferation in bio-engineered whole organ constructs, Biomaterials 52 (2015) 103–112.
[23] D.B. Frank, et al., Early lineage specification defines alveolar epithelial ontogeny in the murine lung, Proc. Natl. Acad. Sci. U. S. A. 116 (2019) 4362–4371.
[24] B. Treutlein, et al., Reconstructing lineage hierarchies of the distal lung epithelium using single-cell RNA-seq, Nature 509 (2014) 371–375.
[25] Y.J. Hou, et al., SARS-CoV-2 D614G variant exhibits efficient replication ex vivo and transmission in vivo, Science 370 (2020) 1464–1468.
[26] B. Korber, et al., Tracking changes in SARS-CoV-2 spike: evidence that D614G increases infectivity of the COVID-19 virus, Cell 182 (2020) 812–827 e819.
[27] A. Mulay, et al., SARS-CoV-2 Infection of Primary Human Lung Epithelium for COVID-19 Modeling and Drug Discovery, bioRxiv, 2020.
[28] T.N.D. Do, et al., A robust SARS-CoV-2 replication model in primary human epithelial cells at the air liquid interface to assess antiviral agents, Antivir. Res. 192 (2021) 105122.
[29] B.M. Ter Ellen, et al., Resveratrol and pterostilbene inhibit SARS-CoV-2 replication in air-liquid interface cultured human primary bronchial epithelial cells, Viruses 13 (2021).

[30] P.P. Mehta, V.S. Dhapte-Pawar, Novel and evolving therapies for COVID-19 related pulmonary complications( ), Am. J. Med. Sci. 361 (2021) 557–566.
[31] J.F. Riordan, Angiotensin-I-converting enzyme and its relatives, Genome Biol. 4 (2003) 225.
[32] K. Kuba, et al., A crucial role of angiotensin converting enzyme 2 (ACE2) in SARS coronavirus-induced lung injury, Nat. Med. 11 (2005) 875–879.
[33] X. Ou, et al., Characterization of spike glycoprotein of SARS-CoV-2 on virus entry and its immune cross-reactivity with SARS-CoV, Nat. Commun. 11 (2020) 1620.
[34] W. Li, et al., Angiotensin-converting enzyme 2 is a functional receptor for the SARS coronavirus, Nature 426 (2003) 450–454.
[35] Z.Z. Yu Zhao, Yujia Wang, Yueqing Zhou, Yu Ma, Wei Zuo, Single-cell RNA Expression Profiling of ACE2, the Receptor of SARS-CoV-2, BioRxiv, 2020.
[36] J. Chen, H. Wu, Y. Yu, N. Tang, Pulmonary alveolar regeneration in adult COVID-19 patients, Cell Res. 30 (2020) 708–710.
[37] H.C. Ott, et al., Perfusion-decellularized matrix: using nature's platform to engineer a bioartificial heart, Nat. Med. 14 (2008) 213–221.
[38] M. Ghaedi, et al., Bioengineered lungs generated from human iPSCs-derived epithelial cells on native extracellular matrix, J Tissue Eng Regen Med 12 (2018) e1623–e1635.
[39] S.E. Gilpin, et al., Enhanced lung epithelial specification of human induced pluripotent stem cells on decellularized lung matrix, Ann. Thorac. Surg. 98 (2014) 1721–1729, discussion 1729.
[40] M. Ghaedi, et al., Human iPS cell-derived alveolar epithelium repopulates lung extracellular matrix, J. Clin. Invest. 123 (2013) 4950–4962.
[41] F. Hawkins, et al., Prospective isolation of NKX2-1-expressing human lung progenitors derived from pluripotent stem cells, J. Clin. Invest. 127 (2017) 2277–2294.
[42] Z. Borok, et al., Keratinocyte growth factor modulates alveolar epithelial cell phenotype in vitro: expression of aquaporin 5, Am. J. Respir. Cell Mol. Biol. 18 (1998) 554–561.
[43] R.F. Gonzalez, L. Allen, L. Gonzales, P.L. Ballard, L.G. Dobbs, HTII-280, a biomarker specific to the apical plasma membrane of human lung alveolar type II cells, J. Histochem. Cytochem. 58 (2010) 891–901.
[44] C.E. Barkauskas, et al., Type 2 alveolar cells are stem cells in adult lung, J. Clin. Invest. 123 (2013) 3025–3036.
[45] W.J. Zacharias, et al., Regeneration of the lung alveolus by an evolutionarily conserved epithelial progenitor, Nature 555 (2018) 251–255.
[46] Y. Yamamoto, et al., Long-term expansion of alveolar stem cells derived from human iPS cells in organoids, Nat. Methods 14 (2017) 1097–1106.
[47] D.W. Takahiko Koyama, Jane L. Snowdon, Laxmi parida, emergence of drift variants that may affect COVID-19 vaccine development and antibody treatment, Pathogens 9 (5) (2020), 2020.
[48] M.M. Zhao, et al., Cathepsin L plays a key role in SARS-CoV-2 infection in humans and humanized mice and is a promising target for new drug development, Signal Transduct. Targeted Ther. 6 (2021) 134.
[49] Y.L. Kang, et al., Inhibition of PIKfyve kinase prevents infection by Zaire ebolavirus and SARS-CoV-2, Proc. Natl. Acad. Sci. U. S. A. 117 (2020) 20803–20813.
[50] A.A. Valyaeva, A.A. Zharikova, A.S. Kasianov, Y.S. Vassetzky, E.V. Sheval, Expression of SARS-CoV-2 entry factors in lung epithelial stem cells and its potential implications for COVID-19, Sci. Rep. 10 (2020) 17772.
[51] I. Hamming, et al., Tissue distribution of ACE2 protein, the functional receptor for SARS coronavirus. A first step in understanding SARS pathogenesis, J. Pathol. 203 (2004) 631–637.
[52] H. Mou, et al., Generation of multipotent lung and airway progenitors from mouse ESCs and patient-specific cystic fibrosis iPSCs, Cell Stem Cell 10 (2012) 385–397.
[53] S.X. Huang, et al., Efficient generation of lung and airway epithelial cells from human pluripotent stem cells, Nat. Biotechnol. 32 (2014) 84–91.
[54] S.E. Gilpin, et al., Perfusion decellularization of human and porcine lungs: bringing the matrix to clinical scale, J. Heart Lung Transplant. 33 (2014) 298–308.
[55] H.C. Ott, et al., Regeneration and orthotopic transplantation of a bioartificial lung, Nat. Med. 16 (2010) 927–933.
[56] E.M. William Zacharias, Isolation and culture of human alveolar epithelial progenitor cells, Protoc. Exchange (2018), https://doi.org/10.1038/protex.2018.015.
[57] J.C. Schittny, Development of the lung, Cell Tissue Res. 367 (2017) 427–444.